Proceedings of the ASME 2024
Pressure Vessels & Piping Conference
PVP2024
July 28-August 2, 2024, Bellevue, Washington

PVP2024-122356

EFFECTS OF HYDROGEN ON FATIGUE LIFE PROPERTIES OF COLD-ROLLED METASTABLE AUSTENITIC STAINLESS STEELS WITH ARTIFICIAL DEFECTS

Junichiro Yamabe[1], Kento Hashiguchi[1], Kentaro Wada[2]

[1]Fukuoka University, Fukuoka, Japan
[2]National Institute for Materials Science (NIMS), Tsukuba, Japan

ABSTRACT

It is important to understand the effect of hydrogen on the fatigue properties of materials to ensure the safety and reliability of hydrogen components. In this study, a cold-rolled metastable austenitic stainless steel, JIS-SUS301, with a tensile strength of around 1.3 GPa was prepared and subjected to plane-bending fatigue tests in air at room temperature by using uncharged and H-charged plate specimens with a thickness of 2 mm. A drilled hole or a sharp notch was introduced at the center of the plate specimens to control crack initiation sites. The H-charged specimens were exposed to 100 MPa hydrogen gas at 270°C for 200 h. The results showed that in high-stress amplitude regimes, the fatigue life of the specimens with a drilled hole or a sharp notch was significantly degraded by hydrogen. In contrast, the fatigue limit of the specimens with a drilled hole, which was determined by the critical stress for crack initiation, was not degraded by hydrogen, or was slightly raised, while the fatigue limit of the specimens with a sharp notch, which was determined by the threshold stress for crack propagation, was not affected or was only slightly degraded by hydrogen. Although the effect of hydrogen on the fatigue limit differed between the drilled hole and sharp notch, the difference was not significant.

Keywords: Hydrogen embrittlement; fatigue; austenitic stainless steel; cold rolling; strain-induced martensitic transformation

1. INTRODUCTION

Global warming is a serious issue that must be actively addressed to achieve worldwide carbon neutrality. The recent social demand for environmental conservation has accelerated the research on hydrogen embrittlement (HE), a phenomenon whereby dissolved hydrogen in metals degrades their tensile strength (TS) and ductility. The degree of HE in various metallic materials is generally evaluated via slow strain rate tensile (SSRT) testing [1–13].

The materials used for high-pressure hydrogen components such as hydrogen stations (HSs) and fuel cell vehicles (FCVs) are exposed to high-pressure hydrogen gas at around 100 MPa. Since the ductility of many materials is degraded by hydrogen, Japanese regulations stipulate that only materials that are negligibly embrittled by hydrogen are to be used in high-pressure hydrogen components to ensure safety [14]. In this context, only stable austenitic stainless steels, Types 316 and 316L, with high nickel-equivalent values [15,16] are authorized for use in high-pressure hydrogen gas environments. These austenitic stainless steels are often referred to as nickel-equivalent materials; however, they are low in strength and high in cost. Therefore, to achieve widespread use of HSs and FCVs, there are active discussions on authorizing metastable austenitic stainless steels such as Type 304, which are cheaper than nickel-equivalent materials, for use in hydrogen components [17,18]. However, the yield and tensile strength of these steels are lower than those of carbon and low-alloy steels; therefore, there are still some problems regarding the improvement of hydrogen-compatible materials with higher strength. One of the methods for improving the TS of such metastable austenitic stainless steels is cold-rolling, but the effects of hydrogen and loading direction on the fatigue properties of cold-rolled metastable austenitic stainless steels have not been clarified. Additionally, while the fatigue limit of various steels with a TS lower than 1 GPa such as carbon [19], low-alloy [19,20], and austenitic stainless steels [21] were not degraded by hydrogen, that of high-strength steels with a TS higher than 1 GPa is not clear.

With this background, the present study focused on metastable austenitic stainless steel, JIS-SUS301, with a TS of around 1.3 GPa as an extreme example. Considering that the fatigue failure of high-strength steels often originates from small defects and inclusions, plane-bending fatigue tests were performed at room temperature with uncharged and H-charged specimens of the cold-rolled steel with artificial defects.

2. MATERIALS AND METHODS

2.1 Materials

A cold-rolled metastable austenitic stainless-steel plate, JIS-SUS301-3/4H, with a thickness of 2 mm was prepared. **Table 1** shows the chemical composition of the steel. The nickel-

equivalent value based on Hirayama's equation [15] was 20.7%. Vickers hardness was *HV* = 401 and the strain-induced martensite fraction before fatigue testing was 9%, as measured by a ferrite meter.

TABLE 1: CHEMICAL COMPOSITION [wt.%]

C	Si	Mn	P	S	Cr	Ni
0.09	0.68	1.03	0.031	0.002	17.1	7.1

2.2 Fatigue specimens

The fatigue specimens shown in **Fig. 1** were cut from the raw plate to ensure that the rolling direction was parallel or perpendicular to the loading direction via an electrical discharge machine (EDM). These specimens were referred to as L- and C-direction specimens, respectively. The TS of an uncharged condition was 1,324 MPa for C-direction or 1,303 MPa for L-direction specimens, respectively. The TS of the C-direction specimen was slightly higher than that of the L-direction specimen and a similar tendency was reported by Tatsurai et al. [22]. To control the crack-initiation sites, a drilled hole with a diameter of 0.5 mm and depth of 0.5 mm or a sharp notch with a length of 0.6 mm, width of 0.1 mm and depth of 0.1 mm was introduced at the center of the specimens using a machining center.

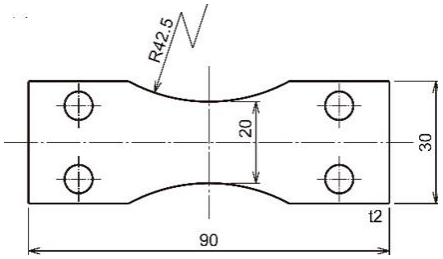

FIGURE 1: SHAPE AND DIMENSIONS OF FATIGUE SPECIMEN IN MM. THE THICKNESS WAS 2 MM.

2.3 Hydrogen-charging conditions

Some of the L- and C-direction specimens were exposed to a high-pressure hydrogen gas environment at 100 MPa and 270°C for 200 h. The hydrogen diffusivity of cold-rolled metastable austenitic stainless steels is closely related to the fraction of strain-induced martensite phases and the value at the fraction of 9% was calculated as approximately 7.7×10^{-12} m^2/s at 270°C [23]. The exposure time required to obtain a uniform hydrogen distribution can be calculated by using L^2/D, where L is the half-thickness of the specimen and D is the hydrogen diffusivity. Since the required time was estimated to be 36 h, an exposure time of 200 h was enough to obtain a uniform distribution of hydrogen in the specimen.

2.3 Fatigue test method

Fatigue tests on uncharged and H-charged specimens were conducted by using a plane-bending fatigue tester in air at room temperature. The stress ratio, R, was −1 and the test frequency, f, was 5 Hz for $<2\times10^6$ cycles or 10–20 Hz for $>2\times10^6$ cycles. The fatigue limit of the specimens with a drilled hole was defined as the maximum stress for non-failed specimens at 2×10^6 cycles under a stress difference of 40 MPa. On the other hand, the fatigue limit of the specimens with a sharp notch was defined as the maximum stress for non-failed specimens at 1×10^7 cycles under a stress difference of 30 MPa. The fatigue tests on some specimens were stopped at specific cycles and their crack initiation and growth behavior were observed.

3. RESULTS AND DISCUSSION

3.1 Residual hydrogen contents

The hydrogen content of some H-charged specimens after the fatigue tests was measured by gas chromatography–mass spectroscopy (GC–MS). The reduction of the hydrogen content after the fatigue tests was at most 3% and hydrogen desorption hardly occurred during the tests. The hydrogen diffusivity at room temperature (23°C) was estimated to be 3.3×10^{-16} m^2/s [23] and the desorption length calculated by $\sqrt{Dt}$, where t is the test time, became 17 μm, which was far smaller than the half-thickness of the specimen. This reveals that almost all the hydrogen remained in the specimens during the tests, corresponding to the experimental hydrogen desorption. Therefore, it was clarified that the hydrogen desorption during the fatigue tests could be ignored.

3.2 Fatigue properties of specimens with drilled hole

3.2.1 Fatigue in high-stress amplitude regimes

Figure 2 shows the *S-N* data of uncharged and H-charged specimens with a drilled hole. For the uncharged specimens, there was a slight difference in the fatigue life between the L- and C-direction specimens in high-stress amplitude regimes such as $\sigma_a \approx 800$ MPa and the fatigue life of the C-direction specimens was slightly longer than that of the L-direction specimens. Uemura et al. [24] reported that in the uncharged condition of cold-rolled copper, the fatigue life of the C-direction specimens was longer than that of the L-direction specimens at high-stress amplitude regimes, which corresponds with the present experimental results.

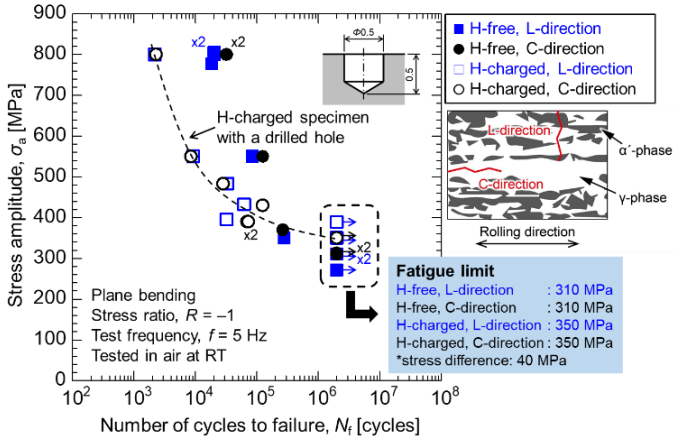

FIGURE 2: *S-N* DATA OF COLD-ROLLED SPECIMENS WITH A DRILLED HOLE.

Figure 3 shows the fracture surface morphology of the L- and C-direction uncharged specimens observed by scanning electron microscopy (SEM). The L-direction specimen with a shorter fatigue life had a relatively flatter fracture surface compared to the C-direction specimen.

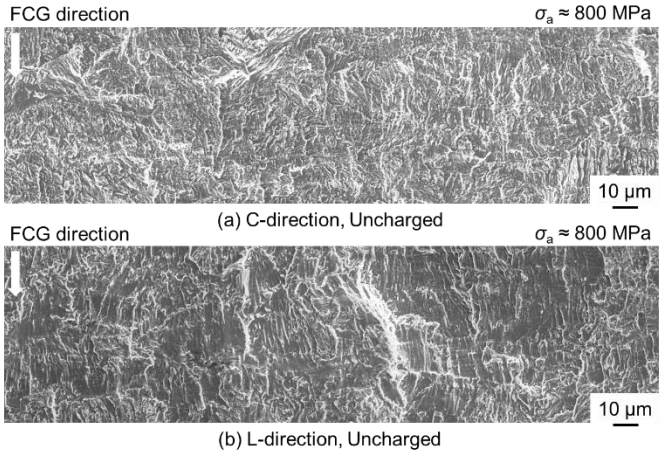

FIGURE 3: FRACTURE SURFACE MORPHOLOGY OF C- AND L-DIRECTION UNCHARGED SPECIMENS TESTED AT STRESS AMPLITUDES OF AROUND 800 MPA.

The fatigue life of the H-charged specimens was around one-tenth of that of the uncharged specimens at $\sigma_a \approx 800$ MPa and additionally, there was no difference in the fatigue life between the L- and C-direction H-charged specimens, unlike that between the L- and C-direction uncharged specimens. **Figure 4** shows the fracture surface morphology of the L- and C-direction H-charged specimens observed by SEM. There was no significant difference in their fracture surface morphology and both specimens showed quasi-cleavage (QC) surfaces.

Figure 5 shows the relationship between the crack length and the number of cycles of the uncharged and H-charged specimens tested at $\sigma_a \approx 800$ MPa. Irrespective of the L- and C-direction conditions, in high-stress amplitude regimes, the fatigue cracks of the uncharged and H-charged specimens were initiated at an early stage of the fatigue cycles and the fatigue life was dominated by the fatigue crack growth (FCG) cycles. Thus, in the uncharged condition, the slight reduction in the fatigue life of the L-direction specimens compared to that of the C-direction specimens was attributed to the difference in their FCG behavior. Uemura et al. [24] stated that the reason for the difference in the fatigue life between the L- and C-direction specimens of the cold-rolled copper was the emergence of fatigue cracks as slip-band cracks along coarse slip bands in the case of the L-direction specimens, suggesting that a difference in the crack path was closely related to the difference in the fatigue life. As shown in **Fig. 3**, the fracture surface of the L-direction uncharged specimen was relatively flatter than that of the C-direction specimen and the difference in these fracture surfaces is presumed to be caused by different FCG paths, as mentioned by Uemura et al. [24]. Since the real FCG length becomes longer with an increase in the rougher fracture surfaces, the formation of such rough fracture surfaces requires a greater number of cycles. A difference in the FCG path is deemed to cause a longer FCG life of the C-direction uncharged specimens compared to that of the L-direction specimens.

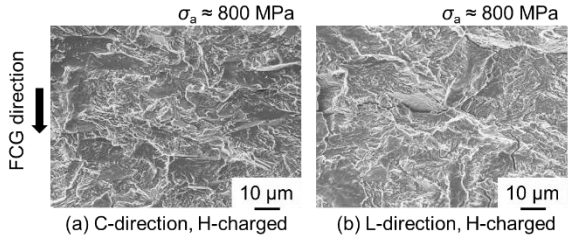

FIGURE 4: FRACTURE SURFACE MORPHOLOGY OF L- AND C-DIRECTION H-CHARGED SPECIMENS TESTED AT STRESS AMPLITUDES OF AROUND 800 MPA.

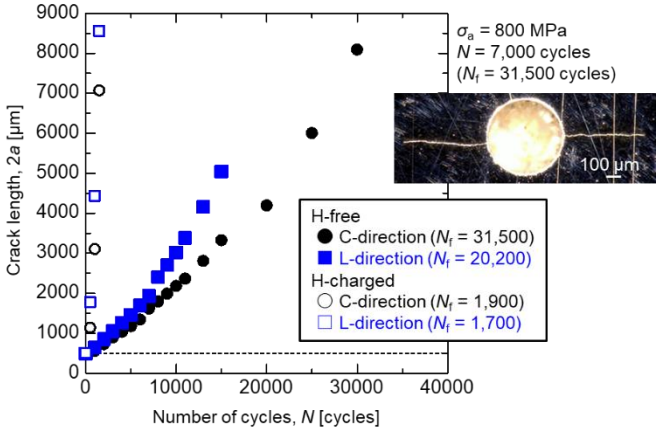

FIGURE 5: CRACK GROWTH BEHAVIOR OF UNCHARGED AND H-CHARGED SPECIMENS.

In contrast, the reduction in the fatigue life by hydrogen was attributed to H-induced acceleration of the FCG rate. The acceleration of the FCG rate by hydrogen accompanied by QC surfaces was observed from solution-treated austenitic stainless steels, Types 304, 316, and 316L, which was explained by the hydrogen-induced successive crack growth (HISCG) model [11]. In this model, slip deformations are localized at the crack tip by hydrogen and so the crack maintains a sharp shape without crack blunting. This model supports the hydrogen-enhanced localized plasticity (HELP) mechanism [25, 26]. It is also deemed that the hydrogen-induced accelerated FCG rate in the present study could be explained by the HISCG model.

3.2.2 Fatigue in low-stress amplitude regimes

In low-stress amplitude regimes, the effects of the loading direction and hydrogen on the fatigue properties became small and the fatigue limit was not degraded by the hydrogen, or was slightly raised, although the present steel had a TS higher than 1 GPa and the fatigue life in high-stress amplitude regimes was degraded by hydrogen. The crack initiation behavior around the

drilled hole of the L- and C-direction uncharged specimens was tested at σ_a = 310 MPa, which is the stress amplitude corresponding to the fatigue limit, and was observed by digital optical microscopy. For the L- and C-direction specimens, nonpropagating cracks were not detected around the drilled hole, inferring that the fatigue limit of the L- and C-direction specimens with a drilled hole was determined by the critical stress for crack initiation. Since the dissolved hydrogen improved the hardness of the steel by about 10% (*HV* = 431), it was deemed that the enhancement of the fatigue limit of the L- and C-direction specimens with a drilled hole was caused by the H-induced increase in hardness.

3.3 Fatigue properties of specimens with a sharp notch

3.3.1 Fatigue in high-stress amplitude regimes

Since the fatigue limit of the specimens with a drilled hole was determined by the critical stress for crack initiation, specimens were prepared with a sharp notch, which had a higher stress concentration than the specimens with a drilled hole. **Figure 6** shows the *S-N* data of uncharged and H-charged specimens with a sharp notch, where the plotted data denoted by * were obtained from the specimens that did not fail at $N = 1\times10^7$ and rested at higher stress amplitudes. According to the stress analysis via the finite element method (FEM), the maximum stress was produced at the notch root located at a depth of 0.1 mm and crack initiation from the notch root was experimentally confirmed. In addition, although some of the H-charged specimens tested at stress amplitudes near the fatigue limit fractured from the specimen edges, no cracks originated from the notch root; therefore, these specimens were regarded as the non-failed ones. The fatigue life behavior of these specimens was similar to that of the specimens with a drilled hole in high-stress amplitude regimes. Namely, the fatigue life of the C-direction specimens was longer than that of the L-direction specimens in the uncharged condition. In contrast, in the H-charged condition, the difference in the fatigue life between the L- and C-direction specimens became small and the fatigue life was degraded by the hydrogen.

3.3.2 Fatigue in low-stress amplitude regimes

The fatigue behavior of the specimens with a sharp notch tested at stress amplitudes around the fatigue limit was different from that of the specimens with a drilled hole; namely, the fatigue limit of the H-charged specimens did not exceed that of the uncharged specimens. Two or more specimens were tested at the same stress amplitude near the fatigue limit and the fatigue limit was determined as the maximum stress amplitude where none of the specimens failed. While the fatigue limit in the uncharged condition was 290 MPa for the L- and C-direction specimens, that in the H-charged condition was 290 MPa for the C-direction specimen and 260 MPa for the L-direction specimen. Despite the H-induced increase in hardness, the fatigue limit of the H-charged specimens with a sharp notch was equal to or slightly lower than that of the uncharged specimens with a sharp notch.

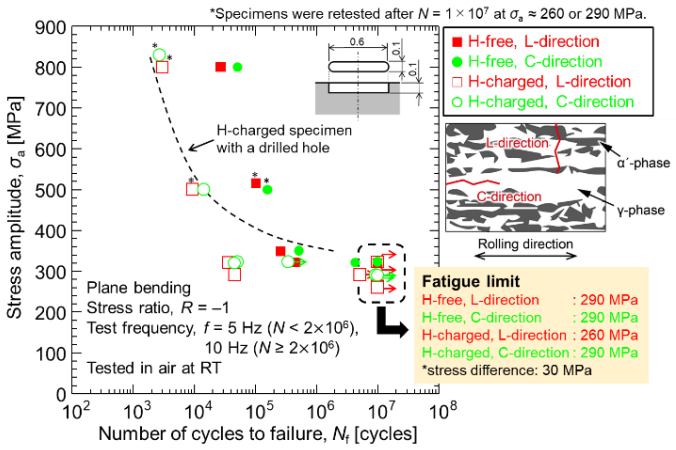

FIGURE 6: *S-N* DATA OF COLD-ROLLED SPECIMENS WITH A SHARP NOTCH.

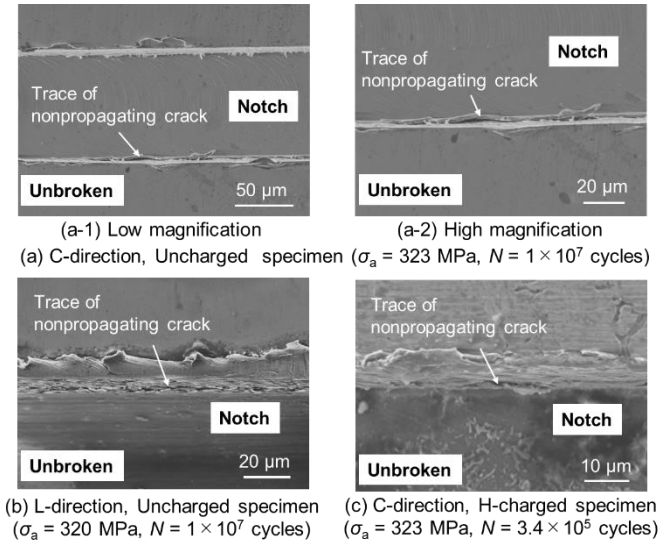

FIGURE 7: CRACK INITIATION BEHAVIOR AROUND SHARP NOTCHES FOR (a) C-DIRECTION UNCHARGED, (b) L-DIRECTION UNCHARGED, AND (c) C-DIRECTION H-CHARGED SPECIMENS TESTED AT A STRESS AMPLITUDE OF 310 MPA, OBTAINED BY USING SEM.

Figure 7 shows the crack initiation behavior of the specimens with a sharp notch tested at a stress amplitude around the fatigue limit and obtained by SEM. The results for the C-direction uncharged specimen, L-direction uncharged specimen, and C-direction H-charged specimen are provided in this figure. The C- and L-direction uncharged specimens did not fail at $\sigma_a \approx 320$ MPa and $N = 1\times10^7$ cycles. Although the C-direction H-charged specimen failed at $\sigma_a \approx 320$ MPa and $N = 3.4\times10^5$ cycles, the fatigue crack originated from the specimen edge, not the sharp notch; therefore, this specimen was regarded as the non-failed one. Cross sections of the specimens having traces of the nonpropagating cracks shown in **Figs. 7(b)** and **7(c)** were also observed by SEM. Cracks initiating from the notch roots were detected; therefore, these could be regarded as the

nonpropagating cracks. This suggests that the fatigue limit of the specimens with a sharp shape was determined by the threshold stress for crack propagation, not the critical stress for crack initiation. This fatigue limit can be considered from the viewpoint of a crack problem based on the fracture mechanics; therefore, the $\sqrt{area}$ parameter model [27] was used for the fatigue limit prediction of the specimens with a sharp notch.

3.4 Positive and negative effects of hydrogen on fatigue limit

According to the $\sqrt{area}$ parameter model [27], the fatigue limit for a specimen with a surface defect can be expressed by using the Vickers hardness, *HV*, and the defect size, $\sqrt{area}$, which is the square root of the projection area of the defect size to the maximum principal stress, as follows:

$$\sigma_{\mathrm{w}} = 1.43(HV + 120)/\left(\sqrt{area}\right)^{1/6} \quad (1)$$

where the units of σ_{w} and $\sqrt{area}$ are MPa and μm, respectively. **Table 2** represents the fatigue limit prediction of the uncharged and H-charged specimens with a sharp notch via the $\sqrt{area}$ parameter model. Errors were calculated by the following equation:

$$\text{Error } [\%] = \frac{\sigma_{\mathrm{w,pre}} - \sigma_{\mathrm{w,exp}}}{\sigma_{\mathrm{w,exp}}} \times 100 \quad (2)$$

where $\sigma_{\mathrm{w,exp}}$ and $\sigma_{\mathrm{w,pre}}$ are the experimental and predicted fatigue limits, respectively. The predicted fatigue limit of the specimens with a sharp notch was the same for both the L- and C-direction conditions, being 294 MPa for the uncharged specimen and 311 MPa for the H-charged specimen, respectively. The fatigue limit of the uncharged specimens could be successfully predicted via the $\sqrt{area}$ parameter model. On the other hand, the experimental fatigue limit of the H-charged specimens was lower by 9–21% than the predicted fatigue limit, although the hydrogen improved the hardness of the specimens. It is known that hydrogen enhances localized slip deformations [11, 23, 24] and restricts strain-induced martensite transformations [28]. There is a possibility that this prevented the improvement of plasticity- and transformation-induced crack closures [29], contributing to a slight decrease in the fatigue limit. The hydrogen caused the increase in hardness, acting as a positive effect on the fatigue limit, and it also caused the suppression of crack closures, acting as a negative effect. It is inferred that the fatigue limit of the H-charged specimens is determined by the superposition of these effects. Nevertheless, although the present steel has a TS higher than 1 GPa and the susceptibility of this material to hydrogen is generally high, the impact of hydrogen on the fatigue limit determined by the threshold stress for crack propagation was small.

TABLE 2: FATIGUE LIMIT PREDICTION VIA THE $\sqrt{area}$ PARAMETER MODEL.

Specimen	*HV*	Experiments, $\sigma_{\mathrm{w,exp}}$ [MPa]	Prediction, $\sigma_{\mathrm{w,pre}}$ [MPa]	Error [%]
C-direction, uncharged	401	290	298	2.7
L-direction, uncharged				
C-direction, H-charged	431	290	315	8.6
L-direction, H-charged		260		21.2

4. CONCLUSION

1. The fatigue life in high-stress amplitude regimes was dominated by the FCG life. The FCG rate was accelerated by hydrogen, leading to a reduction in the fatigue life by the hydrogen. The fracture surface in the presence of hydrogen was covered with quasi-cleavage facets and it was deemed that the H-induced FCG acceleration was attributed to the enhancement of localized slip deformations by hydrogen.
2. The fatigue limit of the specimens with a drilled hole was determined by the critical stress for crack initiation, which was not degraded by the hydrogen, as well as other reported steels with a tensile strength higher than 1 GPa. This fatigue limit was slightly raised by the hydrogen, which was deemed to be attributed to the hydrogen-induced increase in hardness.
3. The fatigue limit of the specimens with a sharp notch was determined by the threshold stress for crack propagation, which was not affected or only slightly degraded by the hydrogen. The hydrogen caused the increase in hardness, acting as a positive effect on the fatigue limit, and caused the suppression of crack closures, acting as a negative effect. It is inferred that the fatigue limit of the H-charged specimens is determined by the superposition of these effects.

REFERENCES

[1] G. Han, J. He, S. Fukuyama, K. Yokogawa, Effect of strain-induced martensite on hydrogen environment embrittlement of sensitized austenitic stainless steels at low temperature, Acta Metall. 46 (1998) 4559–4570.

[2] S. Fukuyama, D. Sun, L. Zhang, M. Wen, K. Yokokawa, Effect of temperature on hydrogen environment embrittlement of type 316 series austenitic stainless steels at low temperature, J. Jpn. I. Met. Mater. 9 (2003) 456–459.

[3] C. San Marchi, B.P. Somerday, X. Tang, G.H. Schiroky, Effects of alloy composition and strain hardening on tensile fracture of hydrogen-precharged type 316 stainless steels, Int. J. Hydrog. Energy 33 (2008) 889–904.

[4] T. Michler, J. Nauman, Hydrogen environment embrittlement of austenitic stainless steels at low temperature, Int. J. Hydrog. Energy 33 (2008) 2111–2122.

[5] T. Michler, A.A. Yukhimchuk, J. Naumann, Hydrogen environment embrittlement testing at low temperatures and high pressures, Corros. Sci. 50 (2008) 3519–3526.

[6] C. San Marchi, T. Michler, K.A. Nibur, B.P. Somerday, On the physical differences between tensile testing of type 304

and 316 austenitic stainless steels with internal hydrogen and in external hydrogen, Int. J. Hydrog. Energy 35 (2010) 9736–9745.

[7] Y. Mine, T. Kimoto, Hydrogen uptake in austenitic stainless steels by exposure to gaseous hydrogen and its effect on tensile deformation, Corros. Sci. 53 (2011) 2619–2629.

[8] T. Michler, C. San Marchi, J. Naumann, S. Weber, Hydrogen environment embrittlement of stable austenitic steels, Int. J. Hydrog. Energy 37 (2012) 6231–6246.

[9] J. Yamabe, S. Matsuoka, Y. Murakami, Surface coating with a high resistance to hydrogen entry under high-pressure hydrogen-gas environment, Int. J. Hydrog. Energy 38 (2013) 10141–1554.

[10] T. Matsuo, J. Yamabe, S. Matsuoka, Effects of hydrogen on tensile properties and fracture surface morphologies of Type 316L stainless steel, Int. J. Hydrog. Energy 39 (2014) 3542–3551.

[11] S. Matsuoka, J. Yamabe, H. Matsunaga, Criteria for determining hydrogen compatibility and the mechanisms for hydrogen-assisted surface crack growth in austenitic stainless steels, Eng. Fract. Mech. 153 (2016) 103–127.

[12] J. Yamabe, O. Takakuwa, H. Matsunaga, H. Itoga, S. Matsuoka, Hydrogen diffusivity and tensile-ductility loss of solution-treated austenitic stainless steels with external and internal hydrogen, Int. J. Hydrog. Energy 42 (2017) 13289–13299.

[13] O. Takakuwa, J. Yamabe, H. Matsunaga, S. Matsuoka, Comprehensive understanding of ductility loss mechanisms in various steels with external and internal hydrogen, Metall. Mater. Trans. A 48 (2017) 5717–5732.

[14] H. Kobayashi, T. Yamada, H. Kobayashi, S. Matsuoka, Criteria for selecting materials to be used for hydrogen refueling station equipment, ASME PVP2016-64033 (2016).

[15] T. Hirayama, M. Ogirima, Influence of chemical composition on martensitic transformation in Fe-Cr-Ni stainless steel, J. Jpn. I. Met. Mater. 34 (1970) 507–510.

[16] S. Takaki, S. Namba, K. Imakawa, A. Macadre, J. Yamabe, H. Matsunaga, S. Matsuoka, Determination of hydrogen compatibility for solution-treated austenitic stainless steels based on a newly proposed nickel-equivalent equation, Int. J. Hydrog. Energy 41 (2016) 15095–15100.

[17] C. San Marchi, J. Yamabe, M. Schwarz, H. Matsunaga, S. Zickler, S. Matsuoka, H. Kobayashi, Global Harmonization of Fatigue Life Testing in Gaseous Hydrogen, ASME PVP2018-84898 (2018).

[18] M. Kimura, N. Yoshikawa, H. Tamura, T. Iijima, A. Ishizuka, J. Yamabe, Test method to establish hydrogen compatibility of materials in high pressure hydrogen gas environment for fuel cell vehicles, ISIJ International 61 (2021) 1333–1336

[19] Y. Ogawa, H. Matsunaga, J. Yamabe, M. Yoshikawa, S. Matsuoka, Fatigue limit of carbon and Cr-Mo steels as a small fatigue crack threshold in high-pressure hydrogen gas, Int. J. Hydrog. Energy 43 (2018) 20133–20142.

[20] H. Matsunaga, M. Yoshikawa, R. Kondo, J. Yamabe, S. Matsuoka, Slow strain rate tensile and fatigue properties of Cr-Mo and carbon steels in a 115 MPa hydrogen gas atmosphere, Int. J. Hydrog. Energy 40 (2015) 5739–5748.

[21] T. Iijima, H. Enoki, J. Yamabe, B. An, Effect of high pressure gaseous hydrogen on fatigue properties of SUS304 stainless steel, ASME PVP2018-84267 (2018).

[22] T. Katsurai, T. Tozawa, H. Kato, Y. Takayama, Fatigue fracture for beam-formed sheet of austenitic stainless steel, Tetsu-to-Hagane 80 (1994) 54–59.

[23] J.-G. Sezgin, D. Takatori, J. Yamabe, Anisotropy of cold-worked Type-304 austenitic stainless steel: focus on the hydrogen diffusivity, Int. J. Hydrog. Energy 44 (2019) 20516–20528

[24] M. Uemura, K. Kigawa, H. Kawabe, T. Yamada, The Directionality of fatigue behavior of cold-rolled copper, J. Jpn. I. Met. Mater. 39 (1975) 298–305.

[25] C.D. Beachem, A new model for hydrogen-assisted cracking (hydrogen “embrittlement”), Metall. Mater. Trans. 3 (1972) 441–455.

[26] H.K. Birnbaum, P. Sofronis, Hydrogen-enhanced localized plasticity—a mechanism for hydrogen-related fracture, Mater. Sci. Eng. A 176 (1994) 191–202.

[27] Y. Murakami, Metal fatigue: Effects of small defects and nonmetallic inclusions (2002) Elsevier.

[28] A. Macadre, T. Tsuchiyama, S. Takaki, Hydrogen-induced increase in phase stability in metastable austenite of various grain sizes under strain, J. Mater. Sci. 52 (2017) 3419–3428.

[29] S. Suresh, R.O. Ritchie, Near-threshold fatigue crack propagation: A perspective on the role of crack closure, The Metallurgical Society of AIME (1984) 227–261.